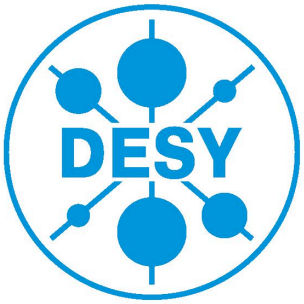

Temperature and Pressure Dependent Properties of Thin Gold Films Grown by Sputter Deposition

Philippa Clark, University of Manchester, UK

September 4, 2013

Abstract

This report outlines the work carried out in the 7 week DESY Summer Student Program 2013, under the supervision of Stephan Roth. This project looked at the growth of gold clusters onto a polystyrene coated silicon substrate via sputter deposition, and in particular how different temperature and pressures of the substrate affected the growth rate and cluster properties. μGISAXS and XRR techniques were used to study the growth, before, during and after sputtering. It was found that the growth rate stays constant for increasing substrate temperature, and increases for increasing pressure, but further analysis is needed to determine exactly how the cluster properties vary during the sputter deposition process.

Contents

1 Introduction

There are many applications of gold in nanotechnology due to its desirable catalytic [1], optical [2], and electronic properties [3]. How these properties depend on the size and form of the gold clusters is fairly well known, so knowing how to grow the exact structures required is an extremely useful aspect.

In this experiment gold nanostructures were grown onto polystyrene via sputter deposition, a relatively slow growth technique where individual gold atoms are adsorbed onto a surface over several minutes. During the sputter deposition *in situ* microbeam grazing incidence small angle x-ray scattering (μGISAXS) measurements were taken. From this data, parts of the reciprocal space scattering pattern were used to determine the form of the gold structures as a function of time. *Ex situ* and x-ray reflectivity (XRR) measurements were also taken, allowing information on film thickness and internal layer properties to be extracted. Access to the internal structures gives these x-ray techniques an advantage over local probe techniques such as scanning electron microscopy. By repeating the sputtering process with the sample held in different conditions, a better understanding of using temperature and pressure to control cluster size (and therefore their properties) was gained.

2 Theory

XRR and μGISAXS are non destructive scattering techniques; both giving a statistical average, over a large area, of the electron density variations on the sample. Here μGISAXS is useful for determining the size and shape of nano structures on a surface, whereas XRR gives more information about the internal layers. Information included in the scattering patterns are structure factor and form factor, which are both important for determining the shape, size, and intercluster distance of the deposited gold. All the information has to be extracted from features of the reciprocal space scattering patterns, which will now be discussed.

2.1 Specular Peak

The x-rays are elastically scattered along the k_f direction (see figure 1), so the scattered wave vector is $\mathbf{q} = (q_x, q_y, q_z)$ where

$$q_x = \tfrac{2\pi}{\lambda}[\cos(\alpha_f)\cos(2\theta_f) - cos(\alpha_i)],$$

$$q_y = \tfrac{2\pi}{\lambda}[\cos(\alpha_f)\sin(2\theta_f)],$$

$$q_z = \tfrac{2\pi}{\lambda}[\sin(\alpha_f) + \sin(\alpha_i)],$$

where λ is the x-ray wavelength and the angles are defined in figure 1. The 2D detector records information in the q_y and q_z directions, where q_z refers to the depth and q_y the in-plane information. The specular peak occurs where the incident angle is equal to the scattered angle; $\alpha_i = \alpha_f$, ie when $q_y = q_x = 0$. $q_y = 0$ corresponds to a realspace distance of ∞, in other words it averages over all height and only depth information of the layers can be gained from the specular peak. Off specular scattering is needed for lateral information.

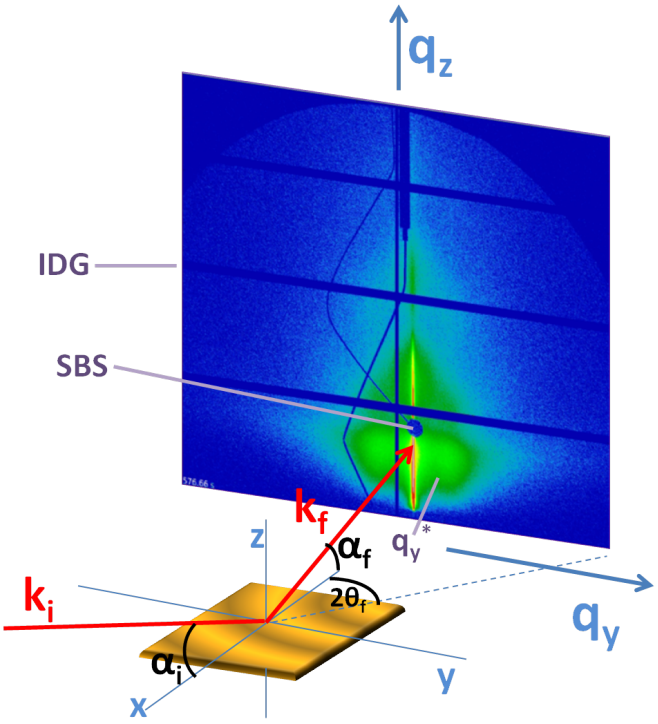

Figure 1: GISAXS geometry, the incoming x-ray with wavevector k_i, at incident angle α_i, is scattered by electron density fluctuations on the sample and becomes k_f, leaving by exit angles $(2\theta_f, \alpha_f)$. The z plane is perpendicular to the substrate surface plane, the x-axis is parallel to the incoming x-ray beam, and the y-axis is perpendicular to that. The figure shows how the recorded reciprocal space corresponds to the real space geometry. Dark lines across the reciprocal surface are the inter detector gaps (IDG), due to the modules of the detectors; it is important to position the image with the important areas not blocked by these gaps. Also indicated is the specular beam stop (SBS), and a yoneda secondary peak position q_y^*.

2.2 Yoneda Peak

A Yoneda peak occurs at $\alpha_f = \alpha_c$, the critical angle. Because α_c is dependent on refractive index (or electron density) it is a material specific peak. Therefore there is a Yoneda peak for each material present in the sample, so in this case 3; one for silicon,

polystyrene and gold. The peak occurs at $q_y = 0, q_z$ corresponding to the critical angle, but when studying the Yoneda peaks a horizontal cut was taken, i.e. $q_y \neq 0$. This lateral intensity information in line (same q_z) with the Yoneda peak can be used to determine structure factor. For example from a secondary intensity peak position, q_y^*; the centre to centre cluster distance $= \frac{2\pi}{q_y^*}$.

2.3 Exsitu detector cut

Once all the gold was deposited, taking another GISAXS image of the sample allows the layer thicknesses to be determined. Because the different layers have different refractive indices, a reflection occurs at each interface e.g. gold-to-polystyrene. These reflections appear as intensity peaks along the specular axis ($q_y = 0$) at different q_z positions, and by taking the difference in q_z values the layer thickness δ can be calculated:

$$\delta = \frac{2\pi}{\Delta q_z}. \tag{1}$$

Once δ and the sputtering time are known, the sputter deposition rate can be calculated. This rate is expected to increase for increasing temperatures.

2.4 XRR

By taking measurements (presputter and postsputter) of increasing α_i and comparing the specular peaks normalised intensities, deviations in electron density can be analysed to give information on roughness, thickness and porosity [4, 5]. Porosity can be calculated by comparing a layers density to that which it should be for a given material; the lower the density the more porous the layer. Of particular interest in this experiment was the overlap layer between gold and polystyrene (see figure 2), and to see how this overlap differs for different temperature sputtering.

3 Experimental Method

3.1 Setup

The ultra-high vacuum sputter chamber was set-up before a pilatus 300K 2D detector in the P03 beamline at the high-brilliance synchrotron light source Petra III storage ring [6], see figure 3 for a simplified diagram of the apparatus setup. The samples used were silicon substrates covered in a (approximately) 50nm layer of polystyrene. A precleaned sample was placed in the x-ray beam of wavelength $\lambda = (0.0957 \pm 0.0001)$nm. The sample-to-detector distance was $D_{SD} = (3518 \pm 2)$mm. The sample was aligned in the microfocus beam with incidence angle $\alpha_i = (0.452 \pm 0.001)^o$. Two lead beamstops were positioned in front of the detector to prevent damage to the detector from the direct (unscattered) and specular beams.

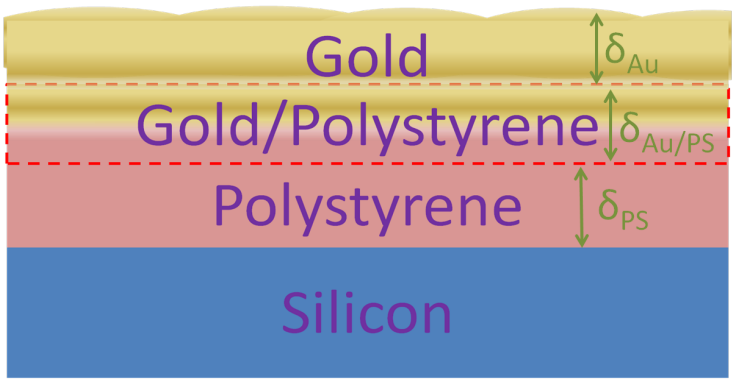

Figure 2: Representation of the samples layers after sputtering is complete. The red enclosed region is the overlap layer between gold and polystrene, the size is exaggerated for this figure. Also indicated in green are the individual layer thicknesses. Not to scale.

3.2 Measurements

First, an XRR scan of the presputter un-coated sample was taken, changing the incidence angle over the range of 0.2-1.2^o in 0.01^o increments. Second, the detector was started recording at 10 frames per second, so that the start of the sputtering process was recorded. The sputtering was started simultaneously with the x-ray shutter opening. The sputtering lasted approximately 610s each time, with 100W power applied. After this, *ex situ* measurements of the sample were taken to allow film thickness information to be extracted. The last stage was taking a second XRR, postsputter, again over the range 0.2-1.2^o in 0.01^o increments.

3.3 Samples overview

Five samples were analysed in total. There were a few differences between samples and the conditions they were sputtered in. For example, the sample MS PS 50 was sputtered at a lower pressure (instead of just different temperature) than the other samples, which could explain the lower sputtering rate. For MS PS 07 only *ex situ* and XRR data was collected, and its sputtering time was estimated from the other samples data. Also MS PS 1 03, whilst still on a silicon substrate, the polymer film consisted of densely packed polystyrene colloids with a nominal diameter of around 100 nm.

4 Analysis and results

The analysis of data was mainly done using dpdak [8], using an image logger to load the data sequence, line integration to select the cuts and the peak fit feature to manually fit Lorentzian curves to the peaks of interest. Once suitable fits were found, the fit information (peak position, intensity, FWHM(full width half maximum)) and errors were extracted for further analysis in other programs. Another feature of dpdak used was the ROI (region of interest) multiplot, used to determine the sputtering period.

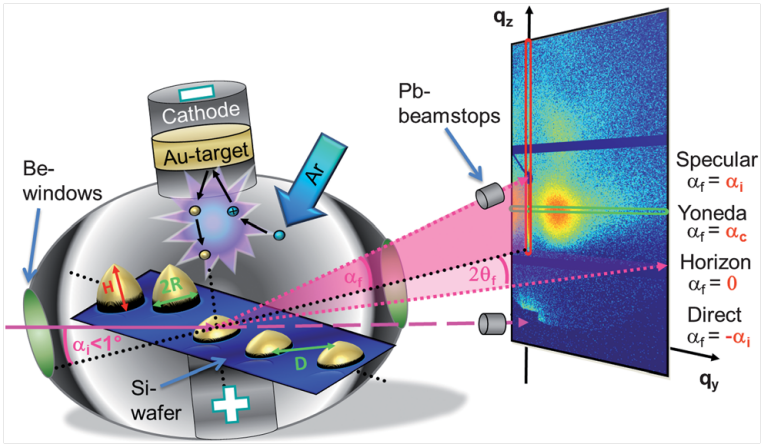

Figure 3: Diagram of the sputter chamber in the μGISAXS setup [7]. α_i denotes the angle between the incident monochromatic X-ray beam and the sample surface, α_f the corresponding exit angle, and $2\theta_f$ the out-of-plane angle. The direct beam position marks the origin of coordinates of the scattering vector components q_y and q_z. The red vertical and green horizontal rectangles represent line cuts; a scattering plane (q_y=0) detector cut and Yoneda cut respectively.

4.1 Exsitu Detector Cut

From an *ex situ* GISAXS image, a detector cut along the specular axis was made, with a width of 5 pixels. Figure 4 shows a typical detector cut from a sputtering at room temperature. Lorentzian curves were fitted to the first two interface reflection peaks; the left fitted peak is due to the air-gold interface, and the second gold-polystyrene. Both Lorentzian curves had to have the same fixed FWHM. The peak on the left is spectral and not of interest for finding film thickness. By using equation 1 and error propagation the real space thickness was calculated for each sample, presented in table 1. The main source of error was determined by how well each Lorentzian fit the data.

4.2 ROI - Determining the Sputtering Period

Using the *in situ* images a 5x5 pixel region was selected just below the specular beam. Then the mean intensity of the selected region was plotted against frame number. From this plot it was clear when the shutters were opened (intensity suddenly increases) and the beginning of the sputtering was determined as where the gradient increases. Similarly for the end of sputtering, the gradient changed again. In most cases it was confirmed that sputtering occurred simultaneously with the shutters opening, but it was still useful to check as a few samples had started sputtering after the shutter opening. The sputtering periods were used to calculate sputtering rate, where rate $= \frac{\delta}{sputteringperiod}$, also presented in table 1.

There seems to be a relation between the sputtering conditions and the growth rate of gold on the sample. By comparing MS PS 02 and MS PS 03 it shows a possible

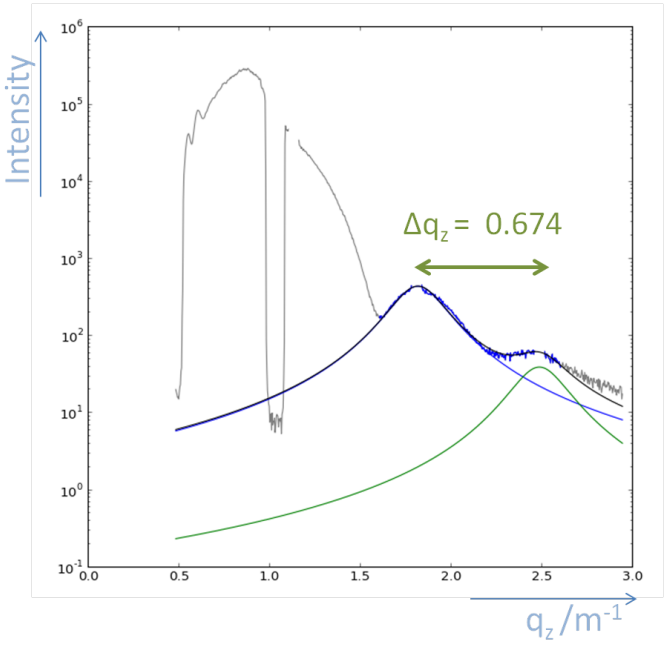

Figure 4: A vertical detector cut from an *ex situ* GISAXS image of a sample sputtered at 28.1^oC.

increase in growth rate due to temperature increase but the overlap in errors is too great to be sure. There appears to be a further increase for MS PS 07, but one cannot be sure without knowing the actual sputter period of this sample. MS PS 50 does not fit this pattern because it had a lower sputtering pressure; hence the drop in growth rate compared to the lower temperature sample MS PS 02. MS PPS 1 03 shows a much higher growth rate than MS PS 02 when they were both grown at room temperature, indicating that 100nm polystyrene colloids are better adsorbers of gold atoms and so a better surface to grow gold on quickly.

Sample Name	Temp. / ^oC	Pressure/$mbar$	Time /s	δ /nm	Rate / nms^{-1}
MS PS 02	28 ± 0.5		612.6 ± 0.1	9.32 ± 0.28	0.0153 ± 0.0005
MS PS 50	50 ± 1		614.0 ± 0.1	6.83 ± 0.26	0.0111 ± 0.0004
MS PS 03	100 ± 5		649.8 ± 0.1	10.30 ± 0.34	0.0159 ± 0.0006
MS PS 07	150 ± 5		611 ± 5	9.70 ± 0.30	0.016 ± 0.005
MS PPS 1 03	28 ± 0.5		612.6 ± 0.1	10.84 ± 0.44	0.0177 ± 0.0007

Table 1: Results of the gold layer thickness, sputtering time and sputter rate for each sample. Please note the discrepancy in sputter rate for MS PPS 1 03 is justified in section 3.3, and the sputter time (and rate) for MS PS 07 is an estimate.

4.3 Yoneda Cuts

The pixel positions for the Si, PS and Au Yoneda peaks were calculated, then a 3 pixel wide horizontal cut was taken. Starting with the last sputtering image, one Lorentzian was fitted to the Yoneda peak (at $q_y = 0$), and then a second Lorentzian was fitted to the $q_y \neq 0$ peak. Sometimes a third Lorentzian was used at $q_y = 0$ if the Yoneda peak showed broadening. An example of a fitted frame is shown in figure 5. The fits were then reused on the rest of the frames. The fits were adjusted and repeated until the 2D colour plot for the fitted curves closely resembled the actual data, see figure 6 for an example of a 2D colour plot fit compared to the original. Once happy with the fit, the fit information and their errors were extracted for calculating cluster distances and size.
Three Yoneda cuts were made instead of just one Au cut because the secondary peaks are better defined in the Si and PS cuts at lower film thicknesses, as can be seen by comparing figures 7,8 and 9. Having all three Yoneda fits gives a better overall picture of how the gold layer grew.

Figure 7, 8 and 9 display the fitted Yoneda 2D plots for Si, PS, and Au respectively for each sample. The second peak (green) appearing at roughly $\delta = 1$nm on most plots represents the gold clusters forming. As the q_y value decreases it means the clusters centres are getting further apart - i.e. the clusters are joining to form larger clusters.
Good comparisons can be made between the MS PS 02 and MS PS 03 (room temperature vs 100^{o}C) plots in figures 7, 8 and 9. In each case the higher temperature sample's second peak decreases more quickly and to a lower q_y value, this is expected as it means the clusters grew faster and larger in the higher temperature conditions. For the exact structures grown more analysis must be done on the extracted peak information. The sample that differs most to the others is always MS PPS 1 03, which was to be expected as it started with different surface structures. Again, further analysis is needed to see exactly how the cluster properties have differed.

4.4 Detector Cut Sequence

A vertical detector cut, width 5 pixels, was made over the entire sputtering sequence. These are displayed for each sample in figure 10. Qualitatively, you can see the higher intensity Yoneda peaks of Si and PS well for lower film thicknesses (lower left of each image), which become less prominent as more gold is deposited and the electron density goes to the bulk value. Above the specular peak (the blocked out area at $q_z = 1$) oscillations can be observed. These are due to the film thickness changing; an increase in film thickness results in more oscillations. The specular beam also broadens with time due to superposition with height oscillations, as $\alpha_i > \alpha_c$, and the oscillations move towards α_i as δ increases.

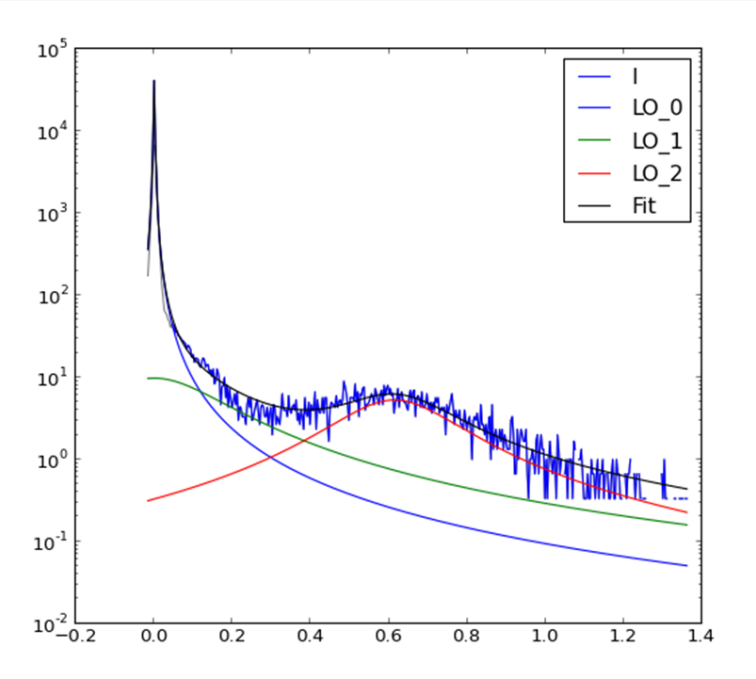

Figure 5: Peak fit display for the PS Yoneda of sample MS PS 02. The blue line is the data, with three Lorentzian curves fitted to it, the overall fit is black.

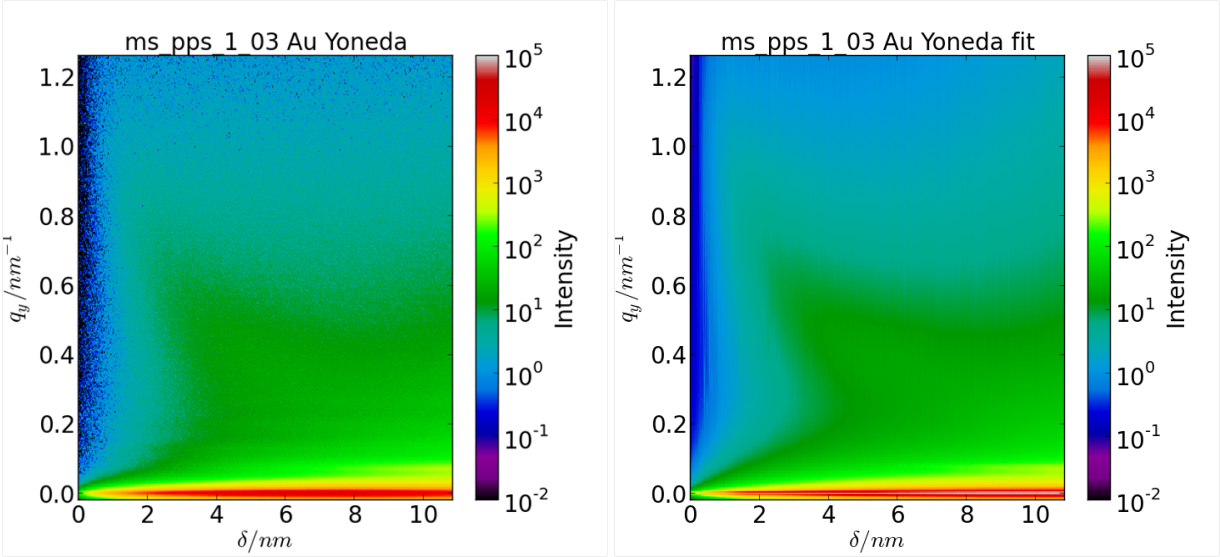

Figure 6: 2D colour plots for a Au Yoneda cut from the MS PPS 1 03 sample. Left shows the original data and the right image is the fitted plot. Film thickness is plotted along the x-axis, set by $0.1 \cdot framenumber \cdot sputterrate$. The colours show intensity, corresponding to the number of photons detected by a pixel during that frames recording.

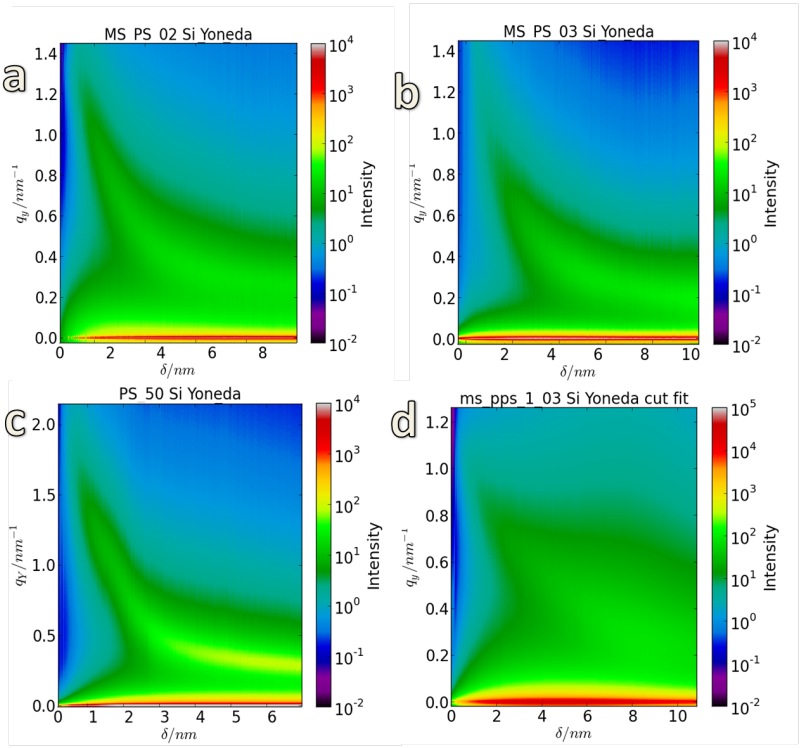

Figure 7: Silicon Yoneda cuts. a-d corresponds to samples MS PS 02, MS PS 03, PS 50, and MS PPS 1 03 respectively.

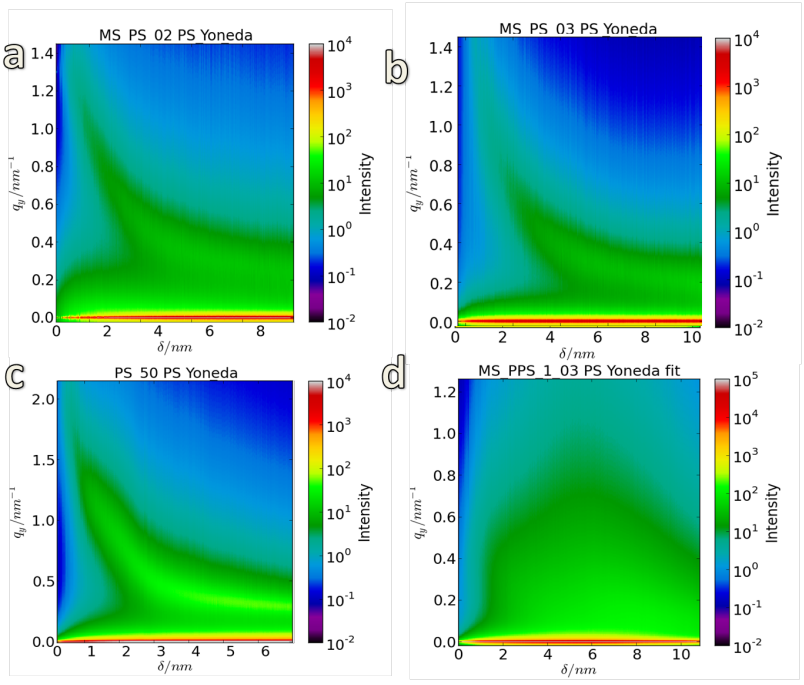

Figure 8: Polystyrene Yoneda cuts. a-d corresponds to samples MS PS 02, MS PS 03, PS 50, and MS PPS 1 03 respectively.

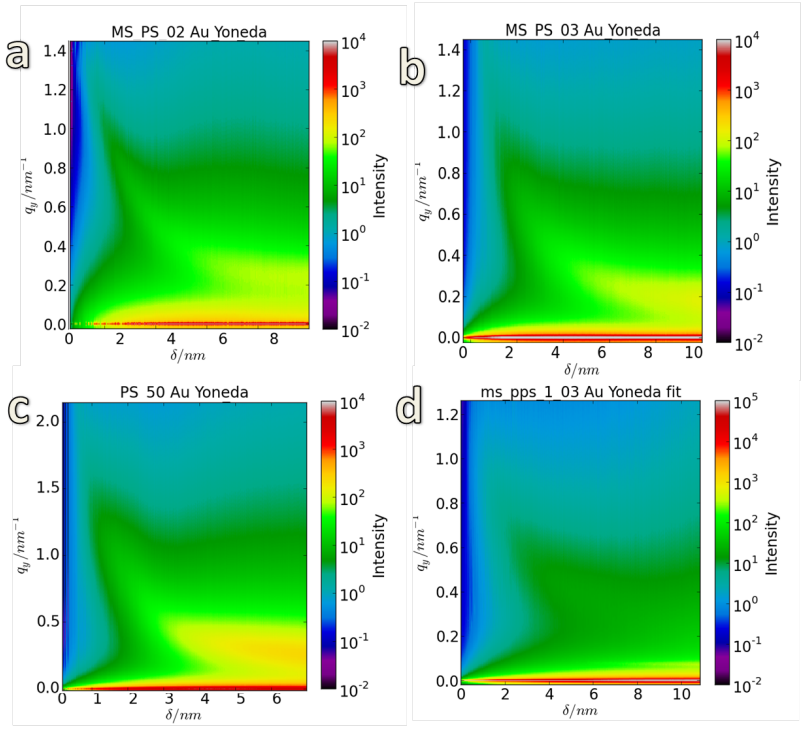

Figure 9: Gold Yoneda cuts. a-d corresponds to samples MS PS 02, MS PS 03, PS 50, and MS PPS 1 03 respectively.

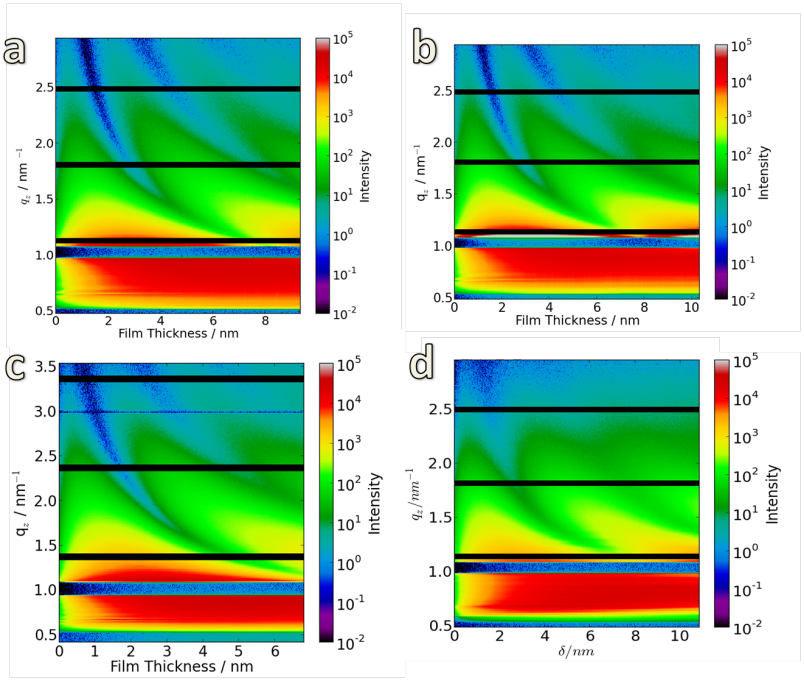

Figure 10: Detector cut sequences. a-d corresponds to samples MS PS 02, MS PS 03, PS 50, and MS PPS 1 03 respectively.

4.5 XRR

The presputter and postsputter XRR data were analysed in the same way. A 5 pixel wide detector cut was taken of the sequence and a single Lorentzian curve was fitted to the specular peak and plotted over increasing angle. A stacked plot was also made of the data, q_z vs intensity, clearly showing the oscillations in intensity for increasing angle. The fitted XRR plots for all 5 samples are shown in figures 11 and 13, and the stacked plots are displayed in figure 12 and 14.

The most obvious change is visible between the stacked plots; where the presputter plots all display regular oscillations over increasing angle, but the postsputter plots each have definite features due to the roughness and porosity of their layers. The exported data from these XRR plots will lead to more information on this, but unfortunately there was not time to finish this part for the report.

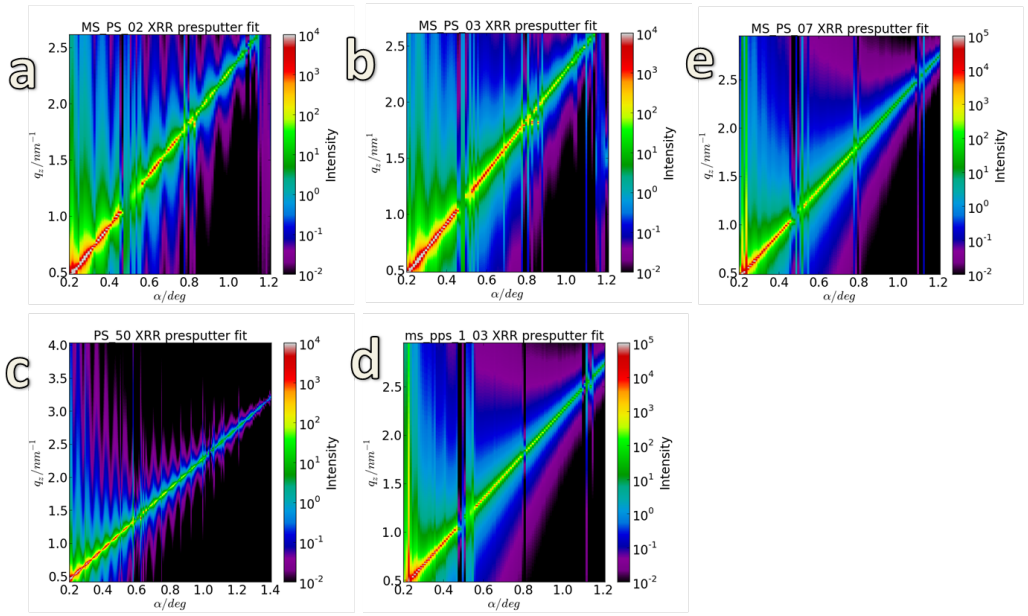

Figure 11: Presputter XRR fits. a-e corresponds to samples MS PS 02, MS PS 03, PS 50, MS PPS 1 03, and MS PS 07 respectively.

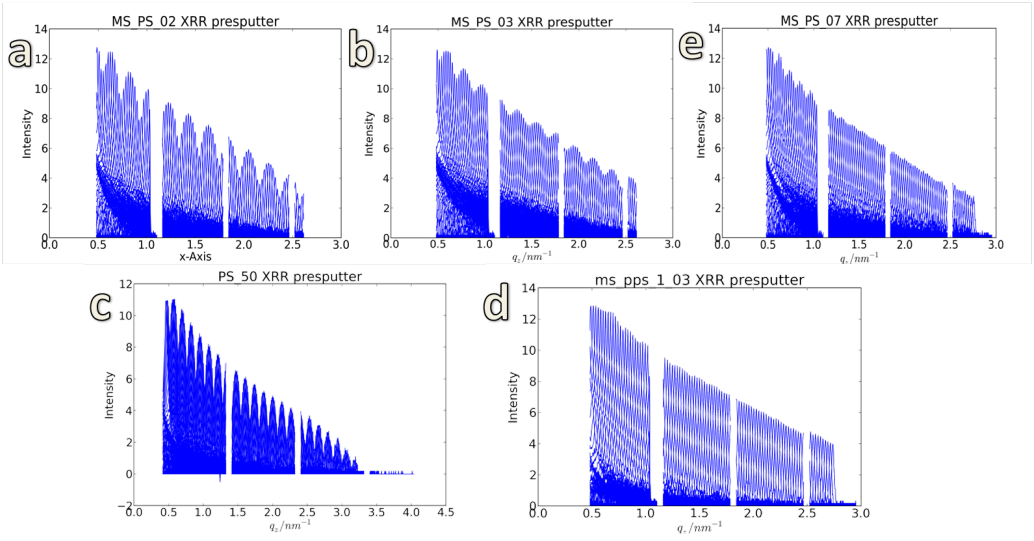

Figure 12: Presputter XRR stacked fits. a-e corresponds to samples MS PS 02, MS PS 03, PS 50, MS PPS 1 03, and MS PS 07 respectively.

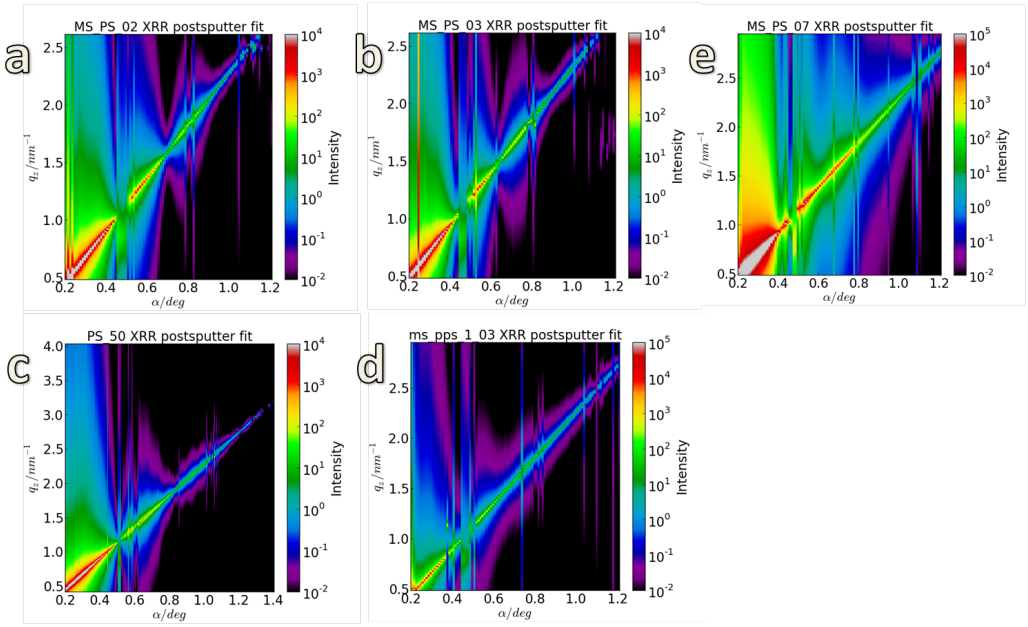

Figure 13: Presputter XRR fits. a-e corresponds to samples MS PS 02, MS PS 03, PS 50, MS PPS 1 03, and MS PS 07 respectively.

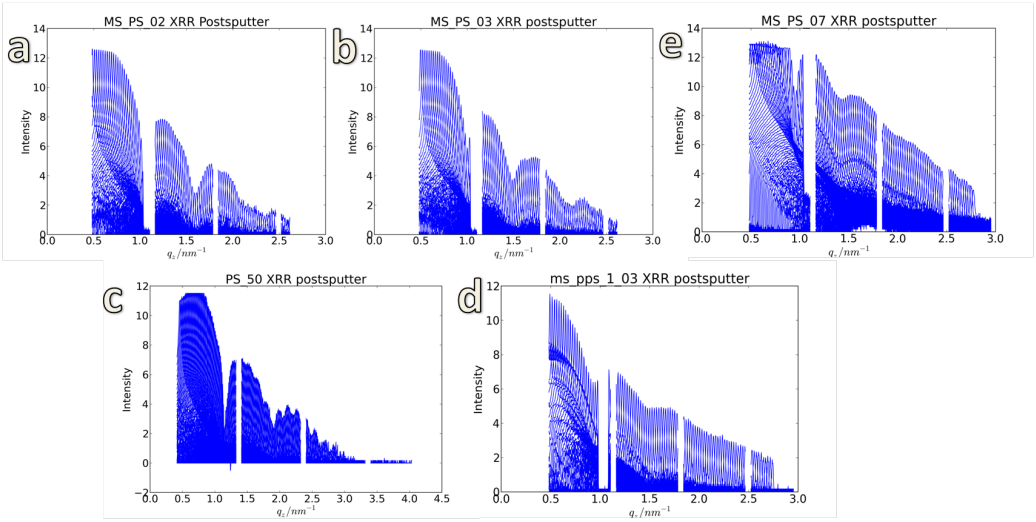

Figure 14: Presputter XRR stacked fits. a-e corresponds to samples MS PS 02, MS PS 03, PS 50, MS PPS 1 03, and MS PS 07 respectively. The distance between intensity minima will be used to estimate the different layer thicknesses.

5 Conclusion

Despite the final stages of analysis not being completed for this data, some assumptions can be made over how different conditions affect the growth of gold onto polystyrene in a sputter chamber. Firstly, that an increase in sputtering temperature appears not to affect the growth rate for gold on a polystyrene thin film. Secondly, an increase in pressure does increase the growth rate. And thirdly, that gold grows faster on polystyrene colloids than just a flat polystyrene surface, but more studies should be done on this to confirm. Only qualitative arguments can be made on the properties of the gold clusters at this stage, so to see exactly how the cluster sizes vary with time, more analysis must be done on the extracted Yoneda fits. Also, to study the gold-polystyrene overlap layer the extracted XRR fits should be further studied.

6 Acknowledgements

I'm extremely grateful to thank Stephan Roth for giving me the opportunity to work in his group, it was a fantastic insight into nano science research and has confirmed that it is this field of physics I wish to work in. I'd like to thank all members of the FS-PE group for allowing me to watch them/help out during beam time. Particular thanks to Matthias Schwartzkopf for guiding me through the project, giving me a lot of his time for explanations and demonstrations, and responding to many, many emails. Last I thank the summer student coordinators for making all this possible, and making sure we enjoyed our time outside of working hours in Hamburg; I've made many great friends and had an awesome summer.

References

[1] T.V. Choudhary and D.W. Goodman (2002), "Oxidation Catalysis by Supported Gold Nano-Clusters" *Topics in Catalysis.*

[2] Gianfranco Carotenuto et al. (2009), "Tuned linear optical properties of gold-polymer nanocomposites" *J*ournal of Materials Chemistry

[3] Yizhong Lu and Wei Chen (2012), "Sub-nanometre sized metal clusters: from synthetic challenges to the unique property discoveries" *Chemical Society Reviews*

[4] Miho Yasaka (2010), "X-ray thin-film measurement techniques" *The Rigaku Journal.*

[5] S. Dourdain et al. (2006), "Determination of porosity of mesoporous silica thin films by quantitative X-ray reflectivity analysis and GISAXS" *Thin Solid Films.*

[6] A. Buffet et al. (2012), "P03, the microfocus and nanofocus X-ray scattering (MiNaXS) beamline of the PETRA III storage ring: the microfocus endstation" *Journal of Synchrotron Radiation.*

[7] M. Schwartzkopf et al. (2013), "From atoms to layers: in situ gold cluster growth kinetics during sputter deposition" *Nanoscale.*

[8] G. Benecke (2013), dpdak, http://www.desy.de/beneckeg/dpdak/